Effect of defects on fracture strength of graphene sheets

M.C. Wang[a], C. Yan[a,*], L. Ma[a], N. Hu[b], M.W. Chen[c]

[a]*School of Engineering Systems, Queensland University of Technology, 2 George Street, GPO Box 2434, Brisbane, Australia*

[b]*Department of Mechanical Engineering, Chiba University, Inage-ku, Chiba, Japan*

[c]*WPI Advanced Institute for Materials Research, Tohoku University, 2 – 1-1 Katahira, Aoba-ku, Sendai 980 – 8577, Japan*

E-mail Address: c2.yan@qut.edu.au

Abstract

With a hexagonal monolayer network of carbon atoms, graphene has demonstrated exceptional electrical and mechanical properties. In this work, the fracture of graphene sheets with Stone-Wales type defects and vacancies were investigated using molecular dynamics simulations at different temperatures. The initiation of defects via bond rotation was also investigated. The results indicate that the defects and vacancies can cause significant strength loss in graphene. The fracture strength of graphene is also affected by temperature and loading directions. The simulation results were compared with the prediction from the quantized fracture mechanics.

Keywords: graphene, defect, fracture strength, molecular dynamics simulation

1. Introduction

Graphene is attracting increasing research effort since its discovery [1], largely due to its exceptional mechanical and electrical properties. With a hexagonal monolayer network of carbon atoms, graphene shows high electron mobility at room temperature ($250{,}000\ cm^2/Vs$) [1], anomalous quantum Hall effect [2], and extremely high Young's modulus (about $1\ TPa$) and fracture strength ($130\ GPa$). The potential

applications include electrodes, chemical sensors, and graphene-based nanocomposites [3-8]. Graphene can be produced via chemical vapour deposition (CVD) [9], mechanical exfoliation [10], chemical reduction of graphene oxide sheets [11], etc. It has been confirmed the properties of graphene can be modified by chemical functionalization [12-14]. However, both material production processes and chemical treatment may introduce structural defects in graphene, such as Stone-Wales (S-W) type defects (nonhexagonal rings generated by reconstruction of graphenic lattice) [15], single and multiply vacancies, dislocation like defects, carbon adatoms, or accessory chemical groups. Recently, Gorjizadeh et al. [16] demonstrated that the conductance decreases in defective graphene sheets. Pei et al. [17, 18] studied the influence of functionalized groups on mechanical properties of graphene. Banhart et al. [19] reviewed possible structural defects in graphene and their effects and potential applications. Unfortunately, there are very few studies of the effects of defects on mechanical properties of graphene and therefore further work is much needed.

In this paper, we present a molecular dynamics investigation on the initiation of S-W defect, and the influence of different defects on mechanical strength of graphene sheets. The fracture strength predicted from the numerical simulation was compared with the so-called quantized fracture mechanics (QFM) theory.

2. Molecular Dynamics Simulation

To simulate a monolayer graphene sheet, a molecular dynamics (MD) model was built that consists of 800 carbon atoms with geometric dimensions of $A = 42.6\text{Å}$ and $B = 49.2\text{Å}$ as shown in Fig. 1. As confirmed by Zhao et al. [20], the possible model size effect can be largely neglected when the diagonal length is over $5\,nm$. Therefore, the diagonal length of our model (Fig. 1) was chosen as $6.51\,nm$. The tensile load was applied to the graphene sheet along both armchair and zigzag directions. The simulation was conducted at a strain rate of $0.005\,ps^{-1}$ and a time step of $0.001\,ps$. The model was firstly relaxed to a minimum energy state using the conjugate gradient energy minimization. Then, Nose-Hoover thermostat [21, 22] was employed to equilibrate the graphene sheet at a certain temperature with periodic boundary

conditions. The adaptive intermolecular reactive bond order (AIREBO) potential [23] implemented in the software package LAMMPS [24], was used to simulate covalent bond formation and bond breaking. The S-W defects are inaccessible by direct molecular dynamics simulations, in that the kinetic rate of defect initiation for a short time scale is quite small at low temperatures. To overcome the time-scale constraint [25] in simulating the S-W defects, we employed nudged elastic band (NEB) method [26] to evaluate the minimum energy path (MEP) for defect initiation. The MEP is a continuous path in a $3N_{atom}$ -dimensional configuration space (N_{atom} is the number of free atoms). The atomic forces are zero at any point in the $(3N_{atom}-1)$ -dimensional hyperplane perpendicular to the MEP. The energy barrier against S-W defect can be determined by the saddle points on the MEP. In our NEB calculations, two-dimensional geometry was considered. The MEPs in $2N_{atom}$ -dimensional configuration space were determined by 20 equally spaced replicas connected by elastic springs. The calculations converged when the force on each replica was less than $0.03\,eV/\AA$. A continuous MEP was then obtained by polynomial fitting of the discrete MEP [27].

3. Results and discussion

3.1 Validation of MD model

To validate the numerical approach, the fracture strength of a perfect graphene sheet was firstly evaluated. The nominal strain-stress curve at $300\,K$, under tension load along both armchair and zigzag directions is shown in Fig. 2. The fracture strength (engineering stress) along the armchair and zigzag directions is 90 and $105\,GPa$, respectively. In terms of true (Cauchy) stress, the fracture strength is 100 and 126 GPa, and the fracture strain is 0.13 and 0.22, respectively. These values are in agreement with the experimental investigation, i.e., $\sigma_f \approx 130GPa$, and $\varepsilon_f \approx 0.25$ [28] as well as previous numerical simulation [20], proving the validity and accuracy of our numerical model.

3.2 Simulation of S-W defects

In this study, we simulated two types of S-W defects, namely S-W_1 and S-W_2, which are caused by 90° rotation of C-C bonds in different directions, as shown in Fig. 3. With the MEP analysis, it is possible to evaluate the generation of S-W defects from a pristine graphene sheet. As shown in Fig. 4a and Fig. 4b, corresponding to tension strain $\varepsilon = 0.0125$, the energy barrier for S-W_1 defect is $53.9\,eV$, which is slightly lower than that for S-W_2 defect $61.1\,eV$. Fig. 5 shows the variation of energy barriers for generation of S-W_1 and S-W_2 defects with the increase of mechanical strain. The energy barrier for S-W_1 defect is constantly lower than that for S-W_2, regardless of the strain level. This indicates that S-W_1 defect is more kinetically favourable than S-W_2. It is clear that the energy required decreases with increase of strain. Corresponding to the failure strain, the energy barriers for generation of S-W_1 and S-W_2 are $16.8\,eV$ and $28.9\,eV$, respectively. This means that mechanical strain alone cannot help to achieve the athermal limit (energy barrier equals zero) for generation of S-W defects via C-C bond rotation. Therefore, S-W defects are kinetically unfavourable when thermal activation energy is lower than the energy barrier at low temperatures. The kinetic rate of S-W defect initiation (υ) can be estimated by the energy barrier E_{eb}, i.e.

$$\upsilon = af_0 \exp^{-E_{eb}/\kappa T} \quad , \tag{1}$$

where f_0 is attempt frequency (about$10^{13}/s$); κ is Boltzmann's constant and a is the lattice spacing $a = \sqrt{3}r_0$, where $r_0 = 1.42\text{Å}$ is the C-C bond length. It can be seen in Equation 1 that the kinetic rate decreases with increase of energy barrier and decrease of temperature. In contrast, our simulation and previous work [29] all confirm that the mechanical load can trigger bond breaking and promote crack propagation in graphene sheets. As compared to S-W defects, vacancy type defects created via bond breaking is easier to be generated by mechanical loading, in particular at low temperatures. This is similar to the analysis of S-W defect initiation in carbon nanotubes [30].

In this study, the temperature effect on the fracture strength of graphene sheets with S-W defects was evaluated. It can be found in Fig. 6 that the fracture strength

decreases with increasing temperature. Clearly, S-W defects significantly deteriorate the fracture strength of graphene, estimated 21.7% and 45.3% by the S-W_1 and S-W_2 defects, respectively. The strength loss caused by S-W_2 is greater than S-W_1 although the initiation of S-W_1 is relatively easier due to the lower energy barrier.

3.3 Effect of vacancy on fracture strength of graphene

In the temperature range of 500~900 K, the fracture strength of graphene sheet with vacancy was evaluated under tension along the armchair direction. The simulation model with 1, 2, and 3 vacancies is shown in Fig. 7b. Fig. 8 shows the fracture strength σ_f for the graphene sheets with different vacancy number at temperatures 300 K, 500 K, and 900 K. It can be seen that fracture strength decreases with increasing temperature as well as the number of vacancy. For the sheet with 3 vacancies, the fracture strength loss is 37.3%, 40.2% and 42.4%, corresponding to 300, 500 and 900 K, respectively. Therefore, atomic scale defect such as vacancy does play a critical role in dictating the mechanical performance of graphene.

In linear elastic fracture mechanics (LEFM), the well known Griffith's criterion was established through an energy analysis during crack propagation, i.e., the release of potential energy associated with crack propagation being equal to the energy required to create the new crack surfaces ($G_c = 2\gamma_c$). It is still arguable if this continuum-based fracture criterion can be applied to failure analysis in a discrete material structure, such as graphene. Recently, an energy-based quantized fracture mechanics (QFM) theory was proposed by substituting the differentials in Griffith's energy balance equation with finite differences [31]. For a nanostructure with n vacancies, the crack length ($2L$) can be estimated as na, in Fig. 7a. Here, the lattice spacing a is also called fracture quantum. Under mode I loading, the fracture strength σ_f can be expressed as

$$\sigma_f(n) = \sigma_c \sqrt{1+\frac{\rho}{2a}}(1+n)^{-1/2} \quad (n>0) \quad , \tag{2}$$

where σ_c is the strength of ideal material at certain temperature, and ρ is the crack

tip radius. In general, when the crack length $2L$ is much smaller than the sample size, for example, $2L/B<1/10$ (B is the height of the graphene sheet, Fig. 1a), the sample size effect can be neglected. Otherwise, the sample size should be taken into account and Equation 2 can be rewritten as [32],

$$\sigma_f(n)\approx\sigma_c\sqrt{1+\frac{\rho}{2a}}(1+n)^{-1/2}\left[\frac{2B}{\pi L}\tan\left(\frac{\pi L}{2B}\right)\right]^{1/2}\quad(n>0) \tag{3}$$

As mentioned before, our model satisfies the condition $2L/B<1/10$ and therefore the fracture can be estimated using Equation 2. With $n=1$, 2 and 3, and $\rho=0.8a$, the fracture strength is $0.836\sigma_c(n=1)$, $0.683\sigma_c(n=2)$, $0.591\sigma_c(n=3)$, as shown in Fig. 8. There is a good agreement between the QFM prediction and the MD simulation. Hence we can approximately predict the fracture strength of graphene sheets with vacancies at different temperatures using the QFM. In Fig. 8, it can be seen that even few atomic defects such as vacancies can significantly reduce the theoretical fracture strength. Also, the fracture strength is dependent on the temperature. A higher strength is observed at low temperatures. In anticipation of broad application of graphene in a range of nano systems, increasing attention should be paid to minimize its defects at atomic level to maintain desirable mechanical performance and structure integrity. In addition, further work is required to investigate on the effect of functional groups introduced via chemical treatment on the fracture strength of graphene.

4. Conclusions

In this work, defect initiation and its effect on fracture strength of graphene sheets were investigated using MD simulation. The results indicate that increase of temperature and mechanical strain can promote the formation of S-W type defects via bond rotation, particularly S-W_1 defect. At low temperatures, mechanical strain can only lead brittle fracture via bond breaking. Both S-W defects and vacancies can cause significant strength loss in graphene. The fracture strength of graphene is also affected by temperature and chirality. The simulation of fracture strength is in good

agreement with the predicted by the energy-based quantized fracture mechanics.

Acknowledgments

C. Yan acknowledges the support from Queensland International Fellowship.

References

[1] K.S. Novoselov, A.K. Geim, S.V. Morozov, D. Jiang, Y. Zhang, S.V. Dubonos, I.V. Grigorieva, A.A. Firsov, Science. 306 (2004) 666-669.

[2] Y. Zhang, Y.-W. Tan, H.L. Stormer, P. Kim, Nature. 438 (2005) 201-204.

[3] F. Schedin, A.K. Geim, S.V. Morozov, E.W. Hill, P. Blake, M.I. Katsnelson, K.S. Novoselov, Nat. Mater. 6 (2007) 652-655.

[4] X. Li, X. Wang, L. Zhang, S. Lee, H. Dai, Science. 319 (2008) 1229-1232.

[5] J. Wu, H.A. Becerril, Z. Bao, Z. Liu, Y. Chen, P. Peumans, Appl. Phys. Lett. 92 (2008) 263302.

[6] S. Stankovich, D.A. Dikin, G.H.B. Dommett, K.M. Kohlhaas, E.J. Zimney, E.A. Stach, R.D. Piner, S.T. Nguyen, R.S. Ruoff, Nature. 442 (2006) 282-286.

[7] M.A. Rafiee, J. Rafiee, Z. Wang, H. Song, Z.-Z. Yu, N. Koratkar, ACS Nano. 3 (2009) 3884-3890.

[8] M.A. Rafiee, W. Lu, A.V. Thomas, A. Zandiatashbar, J. Rafiee, J.M. Tour, N.A. Koratkar, ACS Nano. 4 (2010) 7415-7420.

[9] P.R. Somani, S.P. Somani, M. Umeno, Chem. Phys. Lett. 430 (2006) 56-59.

[10] A.A. Green, M.C. Hersam, Nano Lett. 9 (2009) 4031-4036.

[11] V. Singh, D. Joung, L. Zhai, S. Das, S.I. Khondaker, S. Seal, Prog. Mater. Sci. 56 (2011) 1178-1271.

[12] F. OuYang, B. Huang, Z. Li, J. Xiao, H. Wang, H. Xu, J. Phys. Chem. C. 112 (2008) 12003-12007.

[13] D.W. Boukhvalov, M.I. Katsnelson, J. Phys-Condens Mat. 21 (2009) 344205.

[14] M. Wu, X. Wu, Y. Gao, X.C. Zeng, Appl. Phys. Lett. 94 (2009) 223111.

[15] A.J. Stone, D.J. Wales, Chem. Phys. Lett. 128 (1986) 501-503.

[16] N. Gorjizadeh, A.A. Farajian, Y. Kawazoe, Nanotechnology. 20 (2009) 015201.

[17] Q.X. Pei, Y.W. Zhang, V.B. Shenoy, Nanotechnology. 21 (2010) 115709.

[18] Q.X. Pei, Y.W. Zhang, V.B. Shenoy, Carbon. 48 (2010) 898-904.

[19] F. Banhart, J. Kotakoski, A.V. Krasheninnikov, ACS Nano. 5 (2010) 26-41.

[20] H. Zhao, K. Min, N.R. Aluru, Nano Lett. 9 (2009) 3012-3015.

[21] W.G. Hoover, Phys Rev. A. 31 (1985) 1695.

[22] S. Nosé, J. Chem. Phys. 81 (1984) 511-519.

[23] S.J. Stuart, A.B. Tutein, J.A. Harrison, J. Chem. Phys. 112 (2000) 6472-6486.

[24] S. Plimpton, J. Comput. Phys. 117 (1995) 1-19.

[25] A.F. Voter, F. Montalenti, T.C. Germann, Ann. Rev. Mater. Res. 32 (2002) 321-346.

[26] H. Jonsson, G. Mills, K.W. Jacobsen, in: B.J. Berne, G. Ciccotti, D.F. Coker (Eds.), Classical and quantum dynamics in condensed phase simulations, World Scientific, Singapore, 1998, p. 385.

[27] G. Henkelman, H. Jónsson, J. Chem. Phys. 113 (2000) 9978-9985.

[28] C. Lee, X. Wei, J.W. Kysar, J. Hone, Science. 321 (2008) 385-388.

[29] S.S. Terdalkar, S. Huang, H. Yuan, J.J. Rencis, T. Zhu, S. Zhang, Chem. Phys. Lett. 494 (2010) 218-222.

[30] T. Dumitrica, M. Hua, B.I. Yakobson, P. Natl. Acad. Sci. USA. 103 (2006) 6105-6109.

[31] N.M. Pugno, R.S. Ruoff, Philos. Mag. 84 (2004) 2829-2845.

[32] H. Zhao, N.R. Aluru, J. Appl. Phys. 108 (2010) 064321-064325.

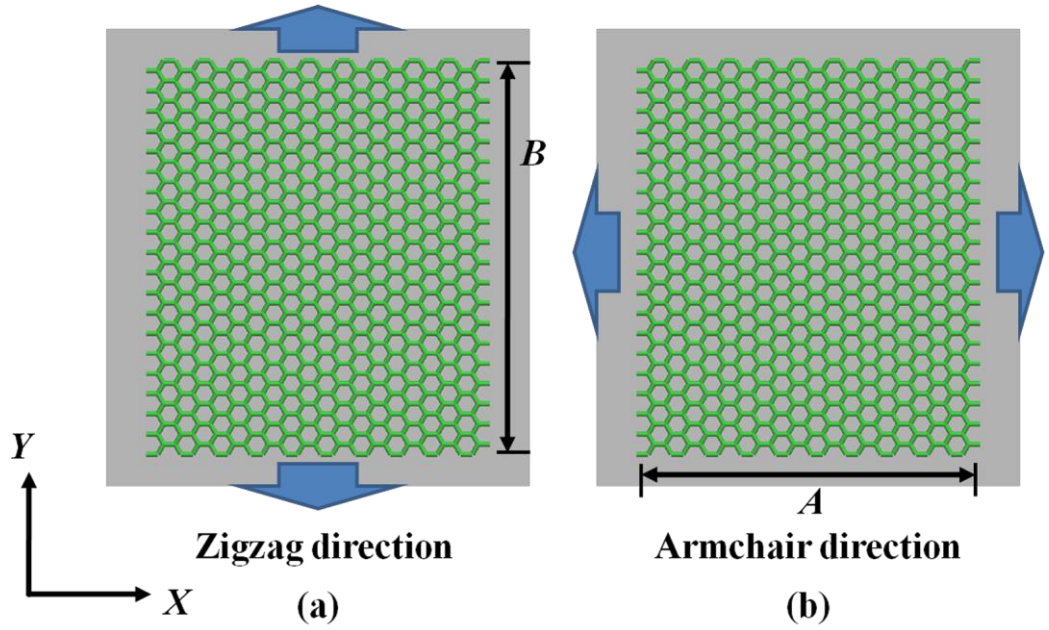

Fig. 1. Simulation models of graphene sheet: uniaxial tension along **(a)** zigzag direction (y axis) and **(b)** armchair direction (x axis).

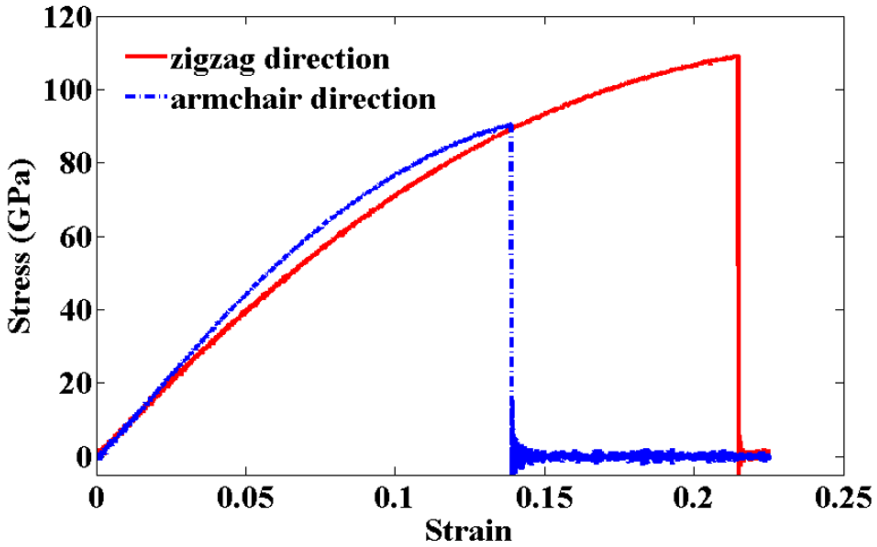

Fig. 2. Nominal stress-strain curves of pristine graphene sheet under unaxial tension along zigzag direction (solid line) and armchair direction (dash-dot line).

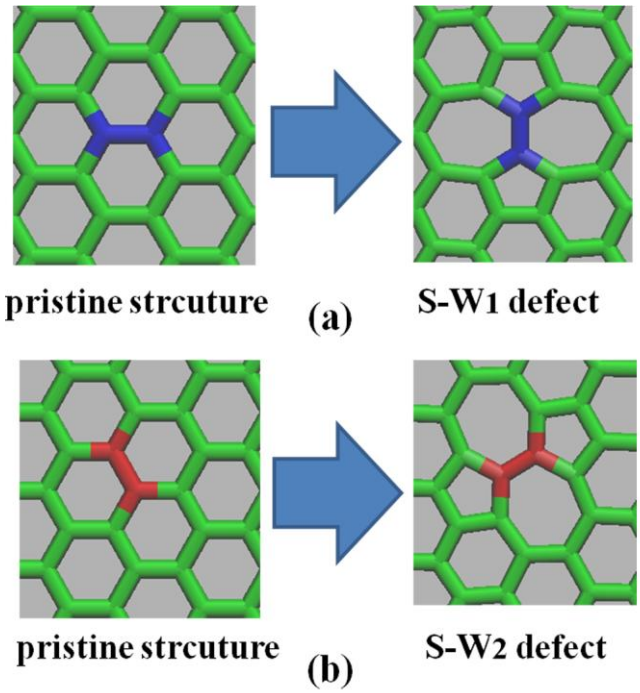

Fig. 3. Two types of Stone-Wales defects: (a) Blue C-C bond rotates by 90° to the S-W_1 defect; (b) Red C-C bond rotates by 90° to the S-W_2 defect.

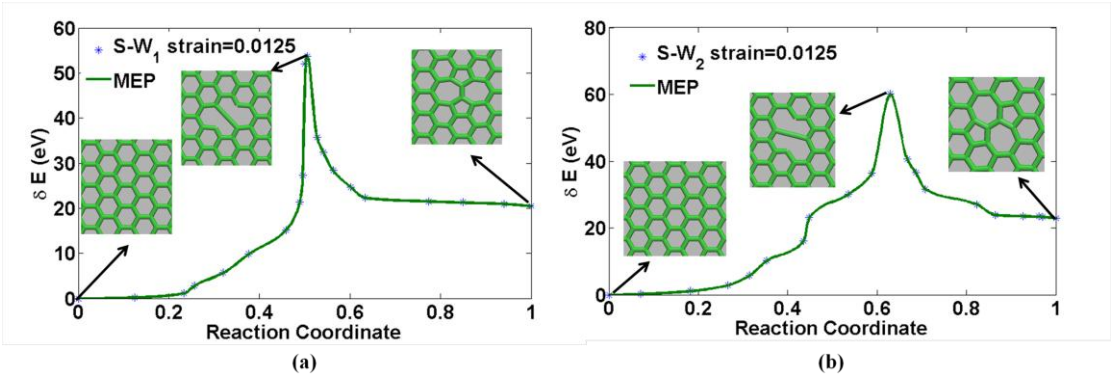

Fig. 4. The minimum energy path (MEP) of **(a)** S-W1 defect initiation and **(b)** S-W2 defect initiation at tension strain $\varepsilon = 0.0125$.

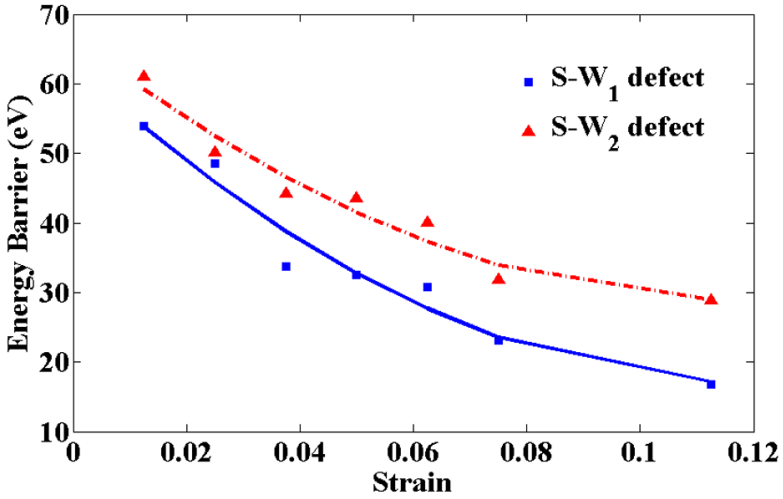

Fig. 5. Energy barriers for S-W1 defect initiation (square point) and S-W2 defect initiation (triangle point) versus tension strain.

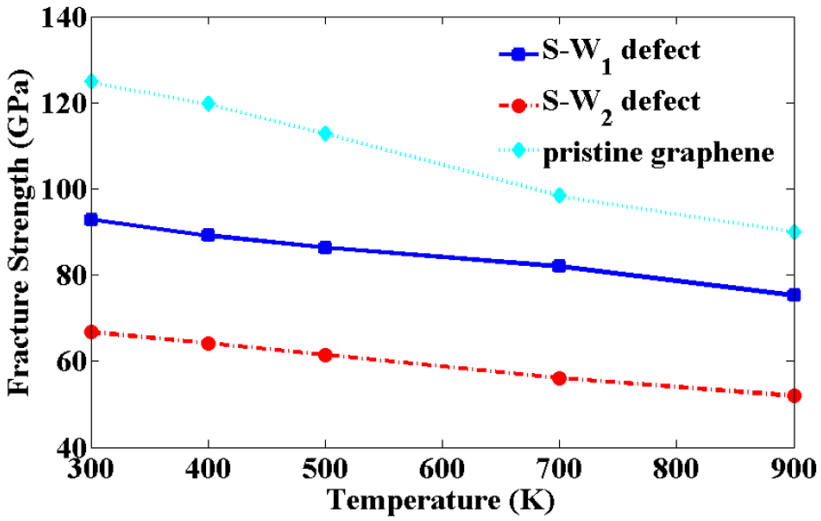

Fig. 4. Fracture strength of pristine graphene (dotted line), S-W_1 defected graphene (solid line) and S-W_2 defected graphene (dash-dot line) versus temperature.

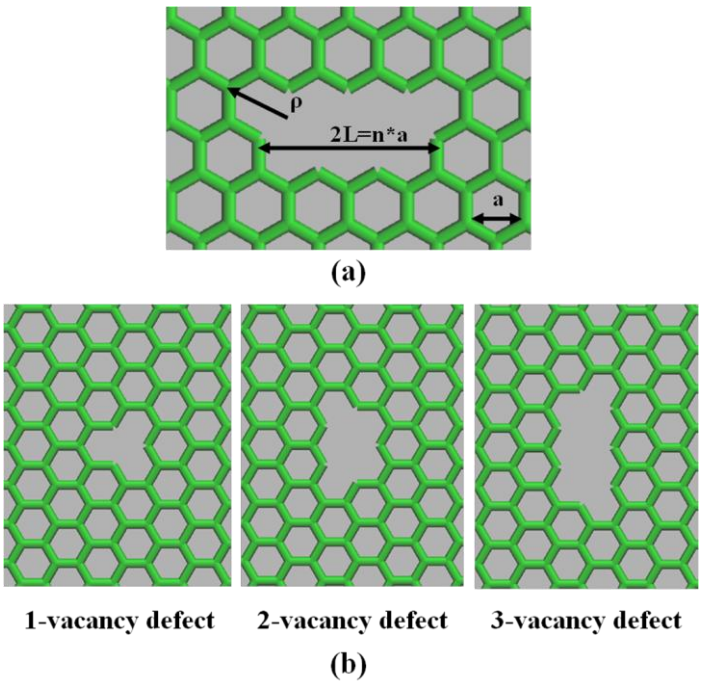

Fig. 7. Graphene sheet with an n-vacancy defect blunt crack: **(a)** In this figure, a is the characteristic fracture quantum; ρ is the tip radius of the crack; $2L = na$ is the crack length. **(b)** 3 types of vacancy defect.

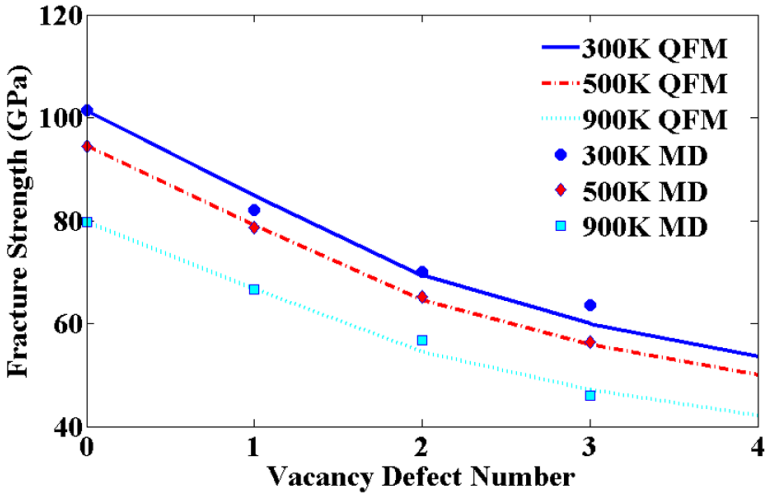

Fig. 8. Fracture strength of defected graphene sheet versus the number of vacancy defect. Solid lines are the results of quantized fracture mechanics (QFM); Points are the results of molecular dynamics (MD) simulations.